K-shell ionization of B, O, and F by 0.4–2.0-MeV He^+ ions

A. Ghebremedhin, W. M. Ariyasinghe, and D. Powers
Department of Physics, Baylor University, Waco, Texas 76798
(Received 15 May 1995; revised manuscript received 8 November 1995)

Absolute *K*-shell ionization cross sections of B, O, and F have been obtained for incident He^+ ion energies of 0.4–2.0 MeV in steps of 0.2 MeV. These ionization cross sections were obtained from Auger-electron yields measured for atomic boron in BF_3; for atomic oxygen in CO, CO_2, and O_2; and for atomic fluorine in $C_2H_2F_2$, C_2F_6, and C_4F_8. For F-containing molecules, the *K*-shell ionization cross sections per atom are found, both in this laboratory and at other laboratories, to decrease as the number of F atoms in the molecule increases. The experimental *K*-shell ionization cross sections are compared to existing experimental *K*-shell ionization cross sections as well as to various theoretical predictions.

PACS number(s): 32.80.Hd, 34.50.Fa

I. INTRODUCTION

K-shell ionization of atoms by charged particles has been the subject of continuing interest for the past two decades. A considerable amount of experimental work has been done by measuring the characteristic x-ray or Auger yields after the production of *K*-shell vacancies by charged particles. Since the *K*-shell fluorescent yields are lower than 1% for second-row elements of the periodic table, an accurate *K*-shell ionization cross section may be obtained by measuring the Auger yields of these elements. Two surveys of experimental *K*-shell ionization cross-section measurements under He^+ ion bombardment have been compiled by Paul and Bolik [1] and by Lapicki [2] to find an empirical formula for *K*-shell ionization cross sections. These compilations reveal that there are a considerable number of experimental measurements for the Auger-electron production yield for the second-row elements C, N, and Ne, but very few corresponding measurements for the elements B, O, and F. For the case of B, only one experimental measurement has been reported, where Kobayashi *et al.* [3] measured the *K*-shell ionization cross section of boron in BF_3 under bombardment of 0.5–2.6-MeV He^+ ions. Their measurements are considerably higher (about 200%) than the perturbed-stationary-state (PSS) theory with energy loss (E), Coulomb deflection (C), and relativistic (R) corrections (ECPSSR) theoretical predictions, but agree fairly closely with the binary-encounter approximation (BEA) theoretical predictions. In a previous experiment [4] at Baylor University, oxygen *K*-shell ionization cross sections were reported that were based on oxygen Auger-electron yields produced by 0.4–2.1-MeV He^+ ion bombardment. These cross sections were found to be 40–50% higher than the ECPSSR theoretical predictions [5]. Kobayashi *et al.* [6] also measured *K*-shell ionization cross sections for oxygen and nitrogen from the *KLL* Auger electrons produced under bombardment of CO_2 and N_2 gases with 0.5–2.6-MeV He^+ ions. They made no comparison with the ECPSSR theory, but found reasonable agreement with the BEA theory. They also reported the *KLL* Auger-electron yield from CCl_2F_2 under the same conditions and found the *K*-shell ionization cross sections to be 50–70% lower than the BEA predictions. McKnight and Rains [7] measured the fluorine *KLL* Auger-electron yield under bombardment of SF_6 gas by 1–5-MeV He^+ ions, and found their *K*-shell ionization cross sections to be 50–60% lower than the BEA theoretical predictions while agreeing closely with the corrected plane-wave Born approximation (CPWBA) theoretical predictions.

The present experiment was undertaken to extend the above measurements to a broader range of gaseous compounds in order to obtain absolute *K*-shell ionization cross sections for B, O, and F in steps of 0.2 MeV under 0.4–2.0-MeV He^+ ion bombardment. Gaseous compounds of B (BF_3), O, (CO, CO_2, and O_2), and F ($C_2H_2F_2$, C_2F_6, and C_4F_8) are used. Since part of the motivation to do the experiment involves an absolute measurement that incorporates a measurement of the efficiency of the Auger-electron detection system, oxygen *K*-shell ionization cross sections reported earlier [4] have been repeated. Any influence from chemical effects is discussed and corrected accordingly.

II. EXPERIMENT

A detailed description of the experimental method is given in Ref. [8]. Briefly, 0.4–2.0-MeV He^+ ions from a Van de Graaff accelerator were magnetically analyzed and directed into an 18-in.-diam. scattering chamber shielded with μ metal and pumped by a Leybold-Heraeus Model TMP-360V turbomolecular pump to the low 10^{-7} Torr region. The scattering chamber contained a negative 100-V bias, parallel-plate electron trap to remove secondary electrons; a 2.36-in.-long, rectangular-shaped differentially pumped gas cell with open end windows (an entrance aperture of 0.039 in. and an exit aperture of 0.047 in.); and a Faraday cup, biased to +45 V, to collect the ion current, which was, typically, 200 nA. Research-grade target gases of BF_3, CO, CO_2, O_2, $C_2H_2F_2$, C_2F_6, and C_4F_8 from Matheson Co., Laporte, Texas, all within minimum purity 99.5% or better, were directed through a gas transport system into the gas cell at an equilibrium pressure of 2.50 mTorr measured by a calibrated Kurt J. Lesker Model TCC-270 thermocouple gauge. Target gas purities were confirmed by an Ametek Residual Gas Analyzer Model MA 100, which was also used to guarantee no air leaks or other gas contamination into the gas system. The Auger electrons exited the gas cell though a 0.039-in.-diam. hole at 90° to the incident ion-beam direction and entered a spherical sector electro-

static analyzer (ESA) from Comstock, Inc., Oak Ridge, Tennessee, operated at a constant 90 eV transmission mode with a resolution of 1.2 eV or better. At the exit port of the ESA was a microchannel plate (MCP) detector with two microchannel plates, Model VUW-8960ES, from Intevac Inc., Palo Alto, California, positioned in a chevron configuration.

In the present experiment, the method of data collection is identical to that in Ref. [8]. The retarding ramp voltages were applied to the ESA to acquire the Auger-electron spectra, which were collected in an EG&G Ortec Model 7150 multichannel analyzer (MCA). These ramp voltages were selected to ensure that each Auger-electron spectrum was collected in the middle portion of the MCA viewing screen with sufficient overlap at the low- and high-energy portions of the spectrum to allow for meaningful background subtraction.

The following procedure, discussed in detail in Refs. [8] and [9], was employed to check for any possible change in the MCP detector efficiency or other parameters through the course of the experiment. First, an Ar LMM Auger-electron yield was measured at 1.0-MeV He^+ ion energy. The argon was removed; the scattering chamber and gas cell were restored to their original vacuum level of low 10^{-7} Torr; one of the target gases for the present experiment was admitted to the gas cell; and its KLL Auger-electron yield was measured as a function of He^+ ion energy. The target gas was then removed, and the cycle was repeated for the Ar LMM Auger-electron yield at the same pressure and He^+ ion current as before to ensure that this yield had not changed from its previous value. This procedure was repeated between every subsequent measurement for the gases in this experiment. No change was allowed that exceeded 3%.

An absolute cross-section determination requires that the target-gas pressure be measured accurately. A Kurt J. Lesker Model TCC-270 thermocouple gauge was mounted at the side of the gas cell, which is positioned at the geometric center of the scattering chamber. A second Model TCC-270 thermocouple gauge was mounted just outside the scattering chamber in the gas-transport line near a needle valve used to ensure a constant gas-flow rate into the cell. In a separate experiment to measure the gas pressure, the same two thermocouple gauges were mounted 1.5 in. apart in a separate T-shaped gas cell and calibrated against each other with N_2 gas pressures from 0 to 70 mTorr; the two measurements were found to agree to within 3%. The gas-cell thermocouple was left in place and the needle-valve thermocouple was replaced with a MKS Baryon Model 221 capacitance manometer. First the gas-cell thermocouple, and then the needle-valve thermocouple, were calibrated against the capacitance manometer initially for N_2 gas, and then separately for each of the gases in the experiment. For gas pressures between 0 and 4.00 mTorr, all pressures for all gases measured with the three gauges were identical within 4%, a finding that is consistent with thermocouple millivolt output versus pressure for O_2, CO_2, and N_2 listed in Ref. [10]. The gas-cell thermocouple output voltage was measured carefully by a parallel arrangement of two resistors, a 1.0 and a 22.1 kΩ, across the thermocouple. The current passing through the 22.1 kΩ resistor was measured with a Keithley Model 485 picoammeter, and the product of this current with the 22.1 kΩ resistance gave the thermocouple output voltage, which was plotted as a function of the thermocouple meter reading. From this thermocouple output voltage, one could determine the pressure inside the gas cell to within 2%. Throughout the course of the Auger-electron cross-section measurements, the needle-valve thermocouple gauge pressure was kept at a predetermined value of 50.0 mTorr, which resulted in a gas-cell thermocouple gauge pressure of 2.50 mTorr for all gases except CO (2.40 mTorr,), CO_2 (2.60 mTorr), and BF_2 (2.00 mTorr). The thermocouple gauge pressure of 50 mTorr at the needle valve, however, was not the same as that of the capacitance manometer, whose readings clustered into two groups: an average value of 57.9 mTorr for the oxygen compounds (O_2, CO_2, and CO) and of 37.3 mTorr for the fluorine compounds ($C_2H_2F_2$, C_2F_6, C_4F_6, and BF_3). The factor of 15 to 23 between the pressure at the supply cylinder and at the gas cell is because (1) of the pressure differential along the connecting lines; (2) the gas cell ''empties'' its gas at a lower pressure through its apertures into the scattering chamber, which is at an even lower pressure; (3) of the sensitivity of the thermocouple on the nature of the gas at pressures greater than 4.00 mTorr; and (4) the rate of efflux through the gas-cell apertures is a function of the mass and size of the molecules. Thus, the leak rate for the smaller oxygen-containing molecules (less mass) is greater than that for the fluorine-containing (greater mass) ones, thereby requiring a higher pressure from the supply cylinder to attain roughly the same pressure in the gas cell. An overall error of 5% has been assigned to the gas-cell pressure measurement on the basis of the gas-cell thermocouple output voltage calibration (2%), the pressure drift during a given Auger-electron measurement (2%), and the difference in measurements among the various pressure gauges for pressures below 4.00 mTorr (4%).

Another important parameter in an absolute cross-section measurement is the determination of the number of He^+ ions that interact with the target gas. Secondary electrons from the He^+ ion beam striking the Faraday cup in the absence of target gas in the gas cell were eliminated by placing a $+45$ V bias on the Faraday cup. This value was selected after a variable voltage from 0 to $+90$ V had been applied to demonstrate that the He^+ ion current remained constant for bias voltages in excess of $+35$ V. A second test involved the measurement of the He^+ ion current at 0.20 MeV intervals from 0.4 to 2.0 MeV with and without each of the seven target gases in the gas cell at 2.50 mTorr pressure. The He^+ ion current was found to increase in the presence of the gas by 3% at 0.4 MeV to 14% at 2.0 MeV for each of the seven gases with a 2% random variation. This increase in the He^+ ion current in the presence of the target gas may be caused by possible charge-changing events in the He^+ ions. Any increase in He^+ ion current at the Faraday cup with gas in the gas cell will mean the collection of fewer Auger electrons in the MCA. This effect was appropriately corrected for each gas by using the fractional increase in charge at each bombarding energy. The total charge collected at the Faraday cup for each Auger-electron spectrum was 7.5×10^{-6} C of He^+ ions, as determined from the corrected integrated current collected at the Faraday cup.

The Auger-electron collection efficiency of the ESA and MCP detector combination was measured as follows. A negatively biased hot filament was placed along the horizontal axis of a 12-in.-long, 1.5-in.-diam. cylindrical copper tube

without end plates. The bias voltage applied to the filament was selected to correspond roughly to the energy of the Auger electrons emitted from boron or oxygen, as will be explained shortly. A Keithley Model 485 picoammeter was used to measure the number of electrons reaching the inner surface of the wall. Since the two ends of the tube were open to the vacuum, a metal ring (1.5-in.-i.d. and 1.2-in.-o.d.) was placed at each end of the tube. The same negative voltage as that applied to the filament was applied to these two metal rings to prevent any electrons from leaving the tube. The outer surface of the tube was well insulated from stray electrons by the application of a thick coating of white Krylon paint. A 0.0625-in.-diam. aperture was drilled in the middle of the side of the horizontal tube, so that the electrons from the filament would go through this aperture directly into the entrance aperture of the ESA and MCP combination in its normal position. All of these devices were housed in the scattering chamber that was evacuated to the low 10^{-7} Torr pressure.

The electron current on the surface of the tube was measured by the picoammeter while the ESA and MCP detector combination was operating at a constant 90 eV transmission energy to record the number of counts in the MCA. If the picoammeter current is I_p, the number of electrons per second recorded by the electron-detecting system is N, the total inner surface area of the tube is A_t, and the counting efficiency of the ESA and MCP combination is ε, then

$$Ne/I_p = \varepsilon A_S/A_t ,$$

where e is the electron charge and A_S is the surface area of the tube that subtends the same solid angle and the solid angle subtended by the entrance aperture of the ESA.

In a previous experiment [8], the transmission efficiency of the ESA was examined as a function of electron energy and found to be monotonically increasing from 76% at 150 eV to 87% at 200 eV to 100% at 350 eV or higher for 90-eV ESA electron transmission energy. The transmission efficiency of the ESA was measured again, but this second time with the hot-wire filament device, where the number of electrons per second was recorded for filament bias voltages from -150 to -450 V (i.e., for 150 to 450 eV electrons) by the electron detection system at 90-eV ESA transmission energy by adjusting the filament current while keeping the picoammeter reading constant. This measurement demonstrated that the number of electrons recorded by the MCA is constant for 350 eV or higher electron energy within a 5% statistical error. Furthermore, the number of electrons recorded by the MCA for 200 and 150 eV electrons were, respectively, 89% and 77% of those at 350 eV. This observation, along with the similar one of the previous experiment, confirms that the ESA-MCP transmission efficiency is constant for electron energies greater than 350 eV, but variable for those lower than 350 eV. Since the average Auger-electron energies of the target atoms in the present experiments are 155 eV (B), 460 eV (O), and 610 eV (F), the efficiency of the ESA-MCP detector combination was studied for 155 and 455 eV electrons using the hot-wire filament device. When this device was biased to -155 V, the electron collection efficiency of the ESA-MCP detector combination was found to be $\varepsilon = 0.35 \pm 0.06$ (17%), which was used to calculate the absolute K-shell ionization cross section of boron. When the device was biased to -455 V, the efficiency of the ESA-MCP detector combination was $\varepsilon = 0.45 \pm 0.06$ (13%), which was used for the absolute K-shell ionization cross sections of oxygen and fluorine. The error assignment of 17% (B) and 13% (O and F) was based on the variation of the picoammeter current reading and on the counting statistics.

Since the ESA-MCP detector combination was exposed to dry nitrogen and to air during the transfer of the detector combination from an Auger-electron detection position to that of an efficiency calibration position, there exists the possibility that the efficiency of the detector combination may have changed during the transfer. An Ar LMM Auger-electron spectrum was measured with 1-MeV He^+ ions, using identical experimental conditions, before and after the efficiency calibration. The two Auger-electron yields agreed to within 6%.

An independent method was employed to verify the efficiency of the electron detection system. A 1-MeV He^+ ion beam was used to produce an Ar LMM Auger-electron spectrum by use of the same procedure explained at the beginning of this section. The number of Auger electrons produced at energies between 200 and 208 eV was recorded by integrating the 200–208 eV energy region of the spectrum. The MCP detector was then dismounted from the ESA and placed in front of the electron aperture from the gas cell. The aperture at the entrance of the MCP detector at this modified location was the same as that used when mounted in the ESA. After a normal vacuum of about 10^{-7} Torr was attained, Ar gas was admitted to the gas cell and the 1-MeV He^+ ion beam was passed through the Ar gas to produce Auger electrons. The number of counts on the MCP detector at this modified location was recorded while the MCP detector entrance was biased first at -200 and then at -208 V. When biased to -200 V, only electrons with energies greater than 200 eV entered the detector. When the bias was -208 V, only electrons with energies greater than 208 eV entered the detector. The difference in these two numbers gives the number of electrons in the energy range 200 to 208 eV. A comparison of this value for the MCP in the modified position to that in its normal position at the detector end of the ESA gives an efficiency of the ESA of 0.58 ± 0.08. Galanti, Gott, and Renaud [11] have reported a MCP efficiency for 200 eV electrons to be about 0.68. The product of the ESA efficiency of 0.58 with the MCP efficiency of 0.68 gives a value of 0.39 ± 0.08, which compares favorably with and confirms the value obtained by the use of the hot-wire filament method. Any drift in MCP detector efficiency caused by exposure to dry nitrogen gas or to air was checked once again by measuring the same Ar LMM Auger-electron spectrum before and after the efficiency calibration with a difference of less than 5% observed between the two Auger-electron yields.

The following sources of error exist in the K-shell ionization cross-section measurements: (1) ESA-MCP detector efficiency calibration (13% for O and F; 17% for B); (2) gas-cell pressure measurement, calibration, and drift (5%); (3) He^+ ion-beam current measurement (2–3%); (4) secondary electron background subtraction in the Auger-electron yields (10%); (5) ESA-MCP efficiency drift during calibration (6%)

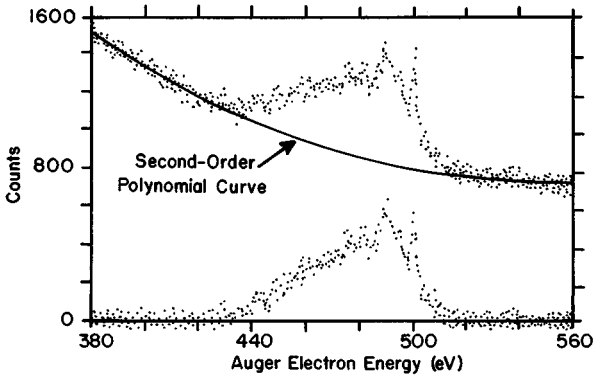

FIG. 1. Oxygen *KLL* Auger-electron spectrum produced by bombardment of CO_2 with 1.2-MeV He^+ ions and recorded at 1.2-eV ESA resolution. The top curve is the spectrum including the background, while the lower curve gives the Auger spectrum after the background has been subtracted.

or during an Auger-electron cross-section measurement (3%); and (6) atmospheric contamination of target gas during any measurement ($<1\%$). These random errors combine in quadrature to give an overall error assignment to the *K*-shell ionization cross-section measurements of 18% for O and F, and 21% for B.

III. RESULTS

A typical *KLL* Auger-electron spectrum of oxygen, produced by 1.2-MeV He^+ ion bombardment of CO_2, is given by the upper portion of Fig. 1. This spectrum is superimposed on the continuous secondary electron background spectrum, which may be subtracted by curve-fitting the lower- and upper-energy ends of the experimental electron spectrum by a suitable polynomial fit. The lower portion of Fig. 1 gives the oxygen *KLL* Auger-electron spectrum after the background has been subtracted. The backgrounds in the oxygen and fluorine Auger-electron spectra were fitted by a second-order polynomial, while a third-order polynomial was used for the boron Auger-electron spectra.

Auger-electron yields were then found by integrating the background-subtracted spectra. These Auger-electron yields were converted to total Auger-electron yields under the assumption that the Auger electrons were emitted isotropically [12], by multiplying by $4\pi/\Delta\Omega$, where $\Delta\Omega$ is the solid angle subtended by the entrance aperture of the ESA at the interaction point between the target gas and the He^+ ion beam. The ESA and MCP detector efficiencies discussed in Sec. II were then used to convert to total Auger-electron cross sections, which are essentially the *K*-shell ionization cross sections.

Since the present objective is to find atomic *K*-shell ionization cross sections, it is necessary to consider molecular-state effects in the measured Auger-electron yields and to correct them accordingly. The effect of the molecular environment on Auger-electron yields has been studied [4,13] previously at Baylor University for a series of carbon-containing molecules, where it was found that carbon *KLL* Auger-electron production in CF_4 was 32% less than that in CH_4. This discovery was interpreted by the loss of carbon *KLL* Auger electrons in terms of their inelastic scattering by the secondary atoms in the molecule, a concept first proposed by Matthews and Hopkins [14]. A calculation based on this decrease of Auger-electron yields from this inelastic scattering is estimated to be 4% for all the oxygen-containing molecules, 5–10% for fluorine-containing molecules, and 17% for boron in BF_3.

The experimental *K*-shell ionization cross sections for boron (BF_3) and oxygen (CO, CO_2, and O_2) as a function of the bombarding He^+ ion energy are given in columns 2–5 of Table I after the above corrections of 17% for boron and 4% for oxygen, respectively, have been made. The numbers in parentheses in the four columns are the experimental *K*-shell ionization cross sections prior to correction for molecular-state effects based on the inelastic-scattering model.

Before discussing the fluorine measurements, it is noticed in the last three columns of Table I that there are no entries at 0.4 and 0.6 MeV. The fluorine *K*-shell ionization cross sections are so low at these He^+ ion energies that the measurements were extremely difficult to make. They are not included in the table because of their extremely large uncertainties.

Given in columns 6–8 of the table are, respectively, the *K*-shell ionization cross sections of fluorine obtained from $C_2H_2F_2$, C_2F_6, and C_2F_8 after the 5–10% correction mentioned above for molecular-state effects. The numbers in parentheses in these columns are the experimental cross sections prior to this correction, and reveal that these uncorrected cross sections *per atom* determined from C_4F_8 are over 50% below those obtained from $C_2H_2F_2$, while those of C_2F_6 are about 30% below those from $C_2H_2F_2$.

The possibility that these differences might be the result of fragmentation effects was then considered. Fragmentation information, compiled and published by National Institute of Standards and Technology (NIST) [15] for use in mass spectroscopic analysis, was used to determine the effective number of fluorine atoms for each fluorine compound. Since fluorine *K*-shell ionization cross sections are tabulated *per fluorine atom*, the cross section *per fluorine atom* will be greater from the fragments than from the parent unfragmented molecule. From the NIST compilation, the major fragments and percentage abundance of each fragment were used to determine the effective number of fluorine atoms, after fragmentation, in C_4F_8, C_2F_6, and $C_2H_2F_2$, to be, respectively, 3.99, 3.16, and 1.5. Thus, dividing the experimental *K*-shell ionization cross section by 3.99 instead of by 8 for C_4F_8, by 3.16 instead of by 6 for C_2F_6, and by 1.5 instead of by 2 for $C_2H_2F_2$, would bring the tabulated fluorine cross sections of the last three columns of Table I into closer agreement. The only problem with this approach is that an independent calculation of the degree of fragmentation under the existing experimental conditions does not support that fragmentation could be the cause for these differences.

This calculation was based upon the following parameters: (1) an ionization cross section [16] for various fragments of C_4F_8 to be of the order of 10^{-16} cm^2, (2) a gas-cell pressure of 2.5 mTorr, which for the gas-cell geometry gives a target-molecule density of 8.0×10^{13} molecules/cm^3; (3) a gas-cell length of 6.00 cm and volume of 1.2 cm^3; (4) an electron current of 1.2×10^9 electrons/sec to produce the fragments in the gas cell based upon an integrated secondary

TABLE I. Boron, oxygen, and fluorine K-shell ionization cross sections in 10^{-20} cm^2/atom produced by 0.4–2.0-MeV He^+ ion bombardment. Numbers in parentheses are the cross sections prior to any chemical state corrections using inelastic scattering (Ref. [14]).

He^+ ion energy (MeV)	Boron	Oxygen			Fluorine		
	BF_3	CO	CO_2	O_2	$C_2H_2F_2$	C_2F_6	C_4F_8
0.4	403±85		5.5±1.0				
	(335)		(5.3)				
0.6	501±105	13.6±2.4	12.2±2.2	9.0±1.6			
	(416)	(13.1)	(11.7)	(8.7)			
0.8	584±123	25.5±4.6	20.0±3.6	19.2±3.5	5.7±1.0		4.5±0.8
	(485)	(24.5)	(19.2)	(18.5)	(5.4)		(4.1)
1.0	640±134	34.3±6.2	33.4±6.0	36.6±6.6	13.5±2.4	9.0±1.6	5.7±1.0
	(531)	(33.0)	(32.1)	(35.2)	(12.8)	(8.2)	(5.2)
1.2	645±135	44.1±7.9	41.1±7.4	52.8±9.5	15.5±2.8	12.2±2.2	7.7±1.4
	(535)	(42.4)	(39.5)	(50.8)	(14.7)	(11.1)	(7.0)
1.4	594±125	50.0±9.0	52.9±9.6	66.8±12.0	19.6±3.5	14.7±2.6	8.5±1.5
	(494)	(48.1)	(50.9)	(64.2)	(18.6)	(13.5)	(7.8)
1.6	580±122	55.1±9.9	76.3±13.7	71.6±12.9	23.7±4.3	15.0±2.7	8.9±1.6
	(481)	(53.0)	(73.4)	(68.8)	(22.5)	(13.6)	(8.1)
1.8	565±119	76.1±13.7	77.8±14.0	77.4±14.0	28.3±5.1	15.7±2.8	9.3±1.7
	(469)	(73.2)	(74.8)	(74.4)	(29.7)	(14.4)	(8.5)
2.0	526±110	62.9±11.3	79.2±14.3	70.0±12.6	27.8±5.0	16.3±2.9	12.6±2.3
	(436)	(60.5)	(76.2)	(67.3)	(26.4)	(14.8)	(11.4)

electron count of 10^6/sec in a typical spectrum such as that in Fig. 1. The calculation gives a number of 6×10^7 fragments/sec produced from the 10^{14} target molecules in the cell. Even the use of a He^+ ion-beam current of 100 nA (6.25×10^{11} ions/sec) would produce only 3×10^8 fragments/sec. What this means is that fragmentation is extremely unlikely to account for the differences in the fluorine K-shell ionization cross sections.

Since neither molecular effects based upon the inelastic scattering model of Matthews and Hopkins [14] nor fragmentation effects seem to account for the difference in the fluorine K-shell ionization cross sections, one must find some other explanation. One possibility is a plausibility argument based upon what is seen by the He^+ ion beam as it produces the KLL Auger electrons in F in different molecular environments. If a single F atom were moving randomly in the gas cell, one would record the KLL Auger-electron yield for this randomly moving atom. When two or more F atoms exist in a molecule, it is to be expected that the He^+ ion beam may not interact with all the F atoms, but only with some fraction thereof. The larger the number of F atoms in the molecule, the less the interaction *per atom* would be. The observed measurements from this laboratory and elsewhere confirm, at least qualitatively, this plausibility approach; namely, there are fewer F atoms in $C_2H_2F_2$ and therefore a higher F cross section per atom. In C_2F_6 and in C_4F_8, the anticipated F cross section per atom would be less than that in $C_2H_2F_2$. In SF_6 measurements made elsewhere, the F cross section per atom is even lower than those obtained here. This approach, however, is purely qualitative, and is offered only as a suggestion.

IV. DISCUSSION

There are three primary theories related to the inner-shell ionization of a target atom by direct Coulombic interaction between the nuclear charge of the projectile with the inner-shell electron of a target atom. These are the binary-encounter approximation (BEA) [17,18], corrected plane-wave Born approximation (CPWBA) [19,20], and perturbed-stationary-state approach with corrections for relativistic, energy loss, and Coulomb-deflection effects (ECPSSR) [21,22].

The BEA theory, first introduced by Garcia [17] and later modified by Hansen [18], predicts a universal curve for all K-shell ionization cross sections regardless of the target, projectile, or incident projectile energy if the K-shell ionization cross section is scaled as $\sigma U_K/Z^2$ against $E/\lambda U_K$, where U_K is the K-shell binding energy of the target-atom electron, Z and E are the atomic number and energy of the projectile, and λ is the projectile mass in units of proton mass. The present experimental K-shell ionization cross sections have been scaled according to the BEA parameters and are presented in Fig. 2 along with measurements by Kobayashi *et al.* [3,6] and of McKnight and Rains [7]. The solid curve is the universal BEA theory and is seen to be systematically lower than 70% of the experimental points. In fact, only the experimental points from F measurements (about 20%) lie below the curve. The BEA, therefore, does not give the best quantitative representation of the experimental results.

The CPWBA theory also predicts a universal curve for K-shell ionization cross sections with a different scaling factor, $(\sigma/\sigma_{0K})(\varepsilon\theta_K/D)$, plotted against $\eta_K/(\varepsilon\theta_K)^2$, where σ is the K-shell ionization cross section, η_K, θ_K, and σ_{0K}

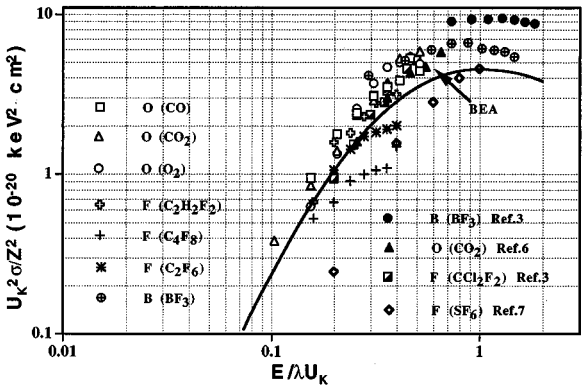

FIG. 2. Experimental K-shell ionization cross sections of boron (BF_3), oxygen (CO, CO_2, and O_2), and fluorine ($C_2H_2F_2$, C_2F_6, and C_4F_8) for MeV He^+ ions, scaled according to the BEA theory (see discussion in text on the BEA parametres). Earlier work of Kobayashi *et al.* (Refs. [3] and [6]) and of McKnight and Rains (Ref. [7]) is also shown. The solid curve represents the BEA theoretical predictions by Hansen (Ref. [18]).

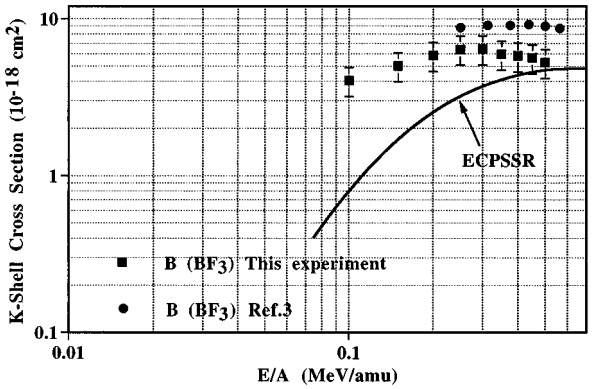

FIG. 4. K-shell ionization cross sections in 10^{-18} cm^2 of boron for MeV He^+ ions. The solid curve is the ECPSSR theoretical prediction (see text for details of theory). The solid squares are the present experimental cross sections for He^+ ions, while the solid circles are the experimental measurements by Kobayashi *et al.* (Ref. [3]) for He^{2+} ions. In both experiments BF_3 was used as the target gas.

are the parameters defined in the theory as follows. $\theta_K = U_K/Z_K^2 R$, where U_K is the K-shell binding energy of the target-atom electron, R is the Rydberg constant, $Z_K = Z - 0.3$ represents the nuclear screening, and Z is the atomic number of the target atom. $\eta_K = (m/M)(E/Z_K^2 R)$, and $\sigma_{0K} = 8\pi a_0^2 Z^2/Z_K^4$, where m and M are, respectively, the electron and projectile mass, E is the projectile energy, a_0 is the Bohr radius, and Z_K and R are defined as before. D and ε, corrections added by Basbas, Brandt, and Laubert [20], to the original plane-wave Born approximation (PWBA) of Merzbacher and Lewis [23], are, respectively, the velocity-dependent factor which enters into the calculated cross sections as an approximate correction for deflection of the projectile by the target nucleus and the factor describing the approximate increase in the K-shell binding energy during the collision. In Fig. 3, the present experimental K-shell ionization cross sections are scaled by the CPWBA parameters and presented along with measurements by Kobayashi *et al.* [3,6] and of McKnight and Rains [7] to the theory. It is clearly seen that the theory predicts the trend of the experimental points quite well on the log-log plot, but is systematically lower. Thus, neither the BEA nor the CPWBA theory faithfully reproduce the experimental measurements.

Finally, the ECPSSR theory, proposed by Brandt and Lapicki [22], is based on the plane-wave Born approximation with hydrogenic wave functions, and is corrected for energy loss of the projectile during the collision (E), for the deceleration and deflection of the projectile in the Coulomb field (C), for the perturbation of the stationary target electron states by the passing projectile (PSS), and for relativistic

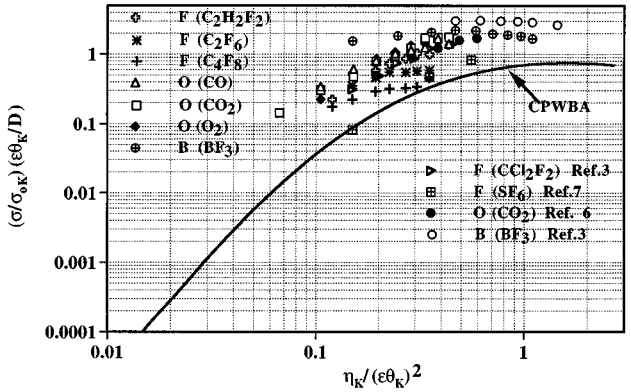

FIG. 3. Experimental K-shell ionization cross sections of boron (BF_3), oxygen (CO, CO_2, and O_2), and fluorine ($C_2H_2F_2$, C_2F_6, and C_4F_8) for MeV He^+ ion bombardment compared to the CPWBA theory (see discussion in text on the CPWBA parameters). The earlier work of Kobayashi *et al.* (Refs. [3] and [6]) and of McKnight and Rains (Ref. [7]) are also shown. The solid curve represents the CPWBA theoretical predictions by Basbas, Brandt, and Laubert (Ref. [19]).

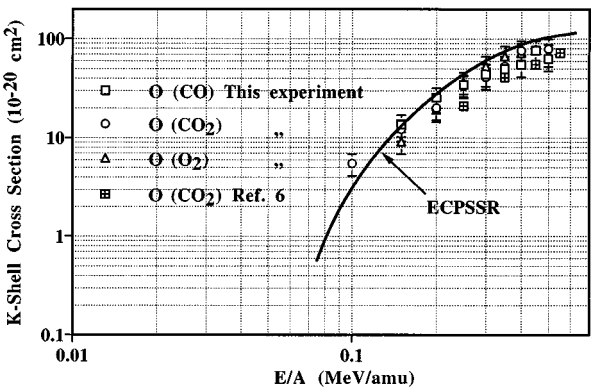

FIG. 5. K-shell ionization cross sections in 10^{-20} cm^2 of oxygen for MeV He^+ ions. The solid curve is the ECPSSR theoretical predictions (see text for details of theory). The open squares, open circles, and open triangles, respectively, are the present experimental cross sections per oxygen atom for He^+ ions using gaseous CO, CO_2, and O_2. The crossed squares are experimental cross sections per oxygen atom by Kobayashi *et al.* (Ref. [6]) for He^{2+} ions in gaseous CO_2.

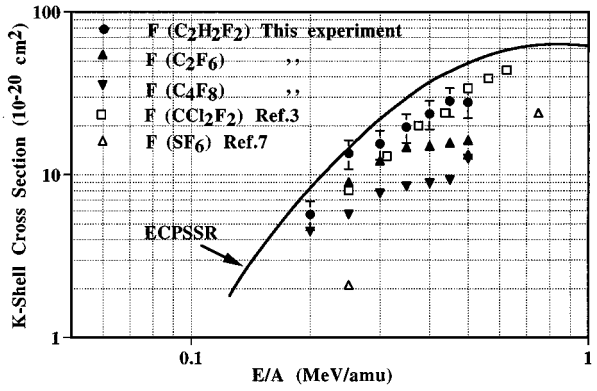

FIG. 6. *K*-shell ionization cross sections in 10^{-20} cm^2 of fluorine for MeV He^+ ions. The solid curve is the ECPSSR theoretical prediction (see text for details of theory). The solid circles, solid triangles, and inverted solid triangles are, respectively, the present experimental cross sections per fluorine atom for He^+ ions using gaseous targets of $C_2H_2F_2$, C_2F_6, and C_4F_8. The open squares are for He^{2+} ions in gaseous CCl_2F_2 by Kobayashi *et al.* (Ref. [3]), and the open triangles are for He^+ ions in gaseous SF_6 by McKnight and Rains (Ref. [7]).

electron motion (R). This theory does not predict a universal curve for ionization cross sections as occurs for the previous two theories. The *K*-shell ionization cross sections as a function of He^+ ion energy per atom per amu are plotted separately for B (Fig. 4), O (Fig. 5), and F (Fig. 6) in order to compare to the ECPSSR theory. The same measurements made elsewhere and given in Figs. 2 and 3 are also plotted in order to compare to the theory. The ECPSSR theory does best for oxygen, but is low for B and high for F.

Figures 4–6 also allow a comparison between the present measurements and those made elsewhere. It is seen in Fig. 4 that the independent boron (BF_3) measurements by Kobayashi *et al.* [3] (closed circles) are 40–70% higher than the present measurements (closed squares). Although this difference is not dramatic, it is possible that a systematic error may exist. On a previous occasion, the Cl *L*-shell ionization cross sections made by Maeda *et al.* [24], performed in the same laboratory as by Kobayashi *et al.* [3], were 200% higher than those measured in this laboratory. It is important to emphasize that the energy of the boron *KLL* Auger electrons is the same as that of the Cl *LMM* Auger electrons, so that a possible systematic error is apparent. However, it is not uncommon [1,2] to find a factor of 2 to 3 difference between the ionization cross-section measurements made at different laboratories in which low-energy Auger electrons are used.

In Fig. 5, it is interesting to see that oxygen *K*-shell ionization cross sections, produced in the present experiment with CO, CO_2, and O_2, are in fair agreement with ECPSSR theoretical predictions for the He^+ ion-energy range 0.4–2.0 MeV. They are also in fair agreement with the measurements for CO_2 by Kobayashi *et al.* [6] at higher He^+ ion energies, but are higher by about 50% than Kobayashi's values at lower He^+ ion energy. The reason for this difference is unknown. It would not likely be the result of a systematic error between the two experiments because of the closer agreement at higher He^+ ion energies. A comparison among the cross-section measurements in the present experiment for CO, CO_2, and O_2 reveals that these three measurements agree within experimental error except at 0.6-MeV He^+ ion energy. The deviation at 0.6 MeV may have been caused by the instability of the He^+ ion beam at this low energy.

Figure 6 also shows that the fluorine *K*-shell measurements from CCl_2F_2 by Kobayashi *et al.* [3] are in close agreement with the present ones from $C_2H_2F_2$, especially at higher values of energy per unit mass E/A. The fluorine values by McKnight and Rains [7] from SF_6, however, are only about 25% of the present fluorine values from $C_2H_2F_2$, and there is no clear explanation for these lower values. Fluorine *K*-shell ionization cross sections obtained from three separate laboratories, however, clearly show values that are systematically lower than the ECPSSR theory.

Thus, none of the three theories, BEA, CPWBA, and ECPSSR, predicts the values for *K*-shell ionization cross sections obtained from three separate laboratories. The best agreement is that of the ECPSSR theory with the oxygen cross sections. All three theories, however, do show general trends, albeit systematically higher or lower (except for oxygen) depending upon the target atom.

The experimental *K*-shell ionization cross sections per atom for boron, oxygen, and fluorine in the present work, as well as that for fluorine from SF_6 by McKnight and Rains [7], were for singly ionized He^+ ions, while the parallel measurements for boron, oxygen, and fluorine by Kobayashi *et al.* [3,6] were for doubly ionized He^{2+} ions. One might anticipate a lower *K*-shell ionization cross section for He^+ than for He^{2+} if the bound electron in He^+ screens the He nuclear charge. The results from Figs. 5 and 6, however, indicate a fair agreement between the He^+ and He^{2+} measurements for oxygen and fluorine. A similar behavior occurred between singly and doubly charged 600-keV He ions in *K*-shell ionization of carbon and CH_4 and C_2H_6 measured, respectively, by Stolterfoht [25] and by Watson and Toburen [26]. However, the boron cross-section measurements by Kobayashi *et al.* [3], where doubly ionized He^{2+} ions were used, are larger ($\approx$40–70%) than the present boron measurements with singly ionized He^+ ions. This difference is not accounted for by the additional electron in the He^+ ion. The following simple argument reveals that there is no effect on *K*-shell ionization of boron from the additional bound electron in He^+. The He ion, whether singly or double ionized, must be sufficiently energetic to penetrate the *K* shell of the target boron atom. 0.6–2.0-MeV He ions are easily able to do this because their velocities are of the same magnitude as the boron *K*-shell electron velocity whose energy is about 205 eV. The Herman and Skillman [27] radius of a He^+ ion is 2.65×10^{-11} m, while that of boron is 0.965×10^{-11} m, with corresponding areas, respectively, 22.2×10^{-22} m^2 and 2.93×10^{-22} m^2. Since the effective area of the He^+ ion is about seven times larger than that of boron, the boron *K* shell will see essentially the doubly charged He^{2+} nucleus of the penetrating He ion, thereby giving a boron *K*-shell ionization cross section that is the same for both He^+ and He^{2+} ions at these MeV energies.

Finally, the absolute experimental *K*-shell ionization cross sections in the present work are based on an efficiency calibration of the ESA and MCP detector combination, as discussed in Sec. II. In the past on two occasions [8,9] relative *L*-shell ionization cross sections from this laboratory have

been reported that were normalized to the 600-keV He^+ ion-induced Ar L-shell ionization cross-section measurements by Stolterfoht, Schneider, and Ziem [28]. As a check of the accuracy of the present K-shell ionization cross sections, the measured Auger-electron yields in the present work were also converted to cross sections by measuring the 600-keV He^+ ion-induced Ar LMM Auger-electron yield and normalizing it to the Ar L-shell ionization cross sections of Stolterfoht *et al.* In this normalization procedure, the efficiency of the MCP detector as a function of the energy of the detected Auger electrons was taken into account and corrected according to the procedure used in Ref. [8]. These K-shell ionization cross sections, based on this relative normalization procedure, were found to be 23% smaller than those listed in Table I for boron, and were 12% smaller than the ones listed for oxygen and fluorine. The larger deviation of boron cross sections determined by this procedure may have been caused by problems encountered with the BF_3 measurement, including possible corrosive effects of the ESA or MCP by the BF_3 gas. It is believed, however, that the absolute measurements are the most reliable and are the ones that should be used.

V. CONCLUSION

Absolute K-shell ionization cross sections have been measured for B, O, and F. The experimental K-shell ionization cross sections per atom of oxygen agree well with the ECPSSR theoretical predictions, while the experimental K-shell ionization cross sections of boron and fluorine are, respectively, higher and lower than the ECPSSR theory. All experimental K-shell ionization cross sections are systematically higher than the CPWBA theory, and the majority of them also exceed the BEA theory. Molecular-state effects based on inelastic scattering of electrons are also considered in all cases. For F, the K-shell ionization cross sections per atom are found, both in this laboratory and at other laboratories, to decrease as the number of F atoms in the molecule becomes larger and larger.

[1] H. Paul and O. Bolik, At. Data Nucl. Data Tables **54**, 75 (1993).

[2] G. Lapicki, J. Phys. Chem. Ref. Data **18**, 111 (1989).

[3] N. Kobayashi, N. Maeda, H. Kojima, S. Akunama, and M. Sakisaka, J. Phys. Soc. Jpn. **47**, 625 (1979).

[4] R. D. McElroy, Jr., W. M. Ariyasinghe, and D. Powers, Phys. Rev. A **36**, 3674 (1987).

[5] H. Paul (private communication).

[6] N. Kobayashi, N. Maeda, H. Hori, and M. Sakisaka, J. Phys. Soc. Jpn. **40**, 1421 (1976).

[7] R. H. McKnight and R. G. Rains, Phys. Rev. A **14**, 1388 (1976).

[8] W. M. Ariyasinghe and D. Powers, Phys. Rev. A **41**, 4751 (1990).

[9] W. M. Ariyasinghe, H. T. Awuku, and D. Powers, Phys. Rev. A **42**, 3819 (1990).

[10] *Methods of Experimental Physics*, Vacuum Physics and Technology, Vol. 14, edited by G. L. Weissler and R. W. Carlson (Academic, New York, 1979), p. 59.

[11] M. Galanti, R. Gott, and J. F. Renaud, Rev. Sci. Instrum. **42**, 1818 (1972).

[12] P. Guo, A. Ghebremedhin, W. Ariyasinghe, and D. Powers, Phys. Rev. A **51**, 2117 (1995).

[13] W. M. Ariyasinghe, R. D. McElroy, Jr., and D. Powers, Nucl. Instrum. Methods B **24/25**, 162 (1987).

[14] D. L. Matthews and F. Hopkins, Phys. Rev. Lett. **40**, 1326 (1978).

[15] Thomas J. Bruno, National Institute of Standards and Technology, Special Publication No. 794, Division of U.S. Dept. of Commerce (U.S. GPO, Washington, D.C., 1990).

[16] M. M. Bibby and G. Carter, Trans. Faraday Soc. **58**, 2455 (1963).

[17] J. D. Garcia, Phys. Rev. A **1**, 280 (1970).

[18] L. S. Hansen, Phys. Rev. A **8**, 822 (1973).

[19] G. Basbas, W. Brandt, and R. Laubert, Phys. Rev. A **7**, 983 (1973).

[20] G. Basbas, W. Brandt, and R. Laubert, Phys. Rev. A **17**, 1655 (1978).

[21] W. Brandt and G. Lapicki, Phys. Rev. A **20**, 465 (1979).

[22] W. Brandt and G. Lapicki, Phys. Rev. A **23**, 1717 (1981).

[23] E. Merzbacher and H. W. Lewis, in *Handbuch der Physik*, edited by S. Flügge (Springer-Verlag, Berlin, 1958), Vol. 34, p. 166.

[24] N. Maeda, N. Kobayashi, H. Hori, and M. Sakisaka, J. Phys. Soc. Jpn. **40**, 1430 (1976).

[25] N. Stolterfoht, D. Schneider, and K. G. Harrison, Phys. Rev. A **8**, 2363 (1973).

[26] R. L. Watson and L. H. Toburen, Phys. Rev. A **7**, 1853 (1973).

[27] F. Herman and S. Skillman, *Atomic Structure Calculations* (Prentice-Hall, Englewood Cliffs, NJ, 1963).

[28] N. Stolterfoht, D. Schneider, and P. Ziem, Phys. Rev. A **10**, 81 (1974).